Chapter 7

The pulsation of the roAp star HR 3831

Some of the results presented in this chapter were published in paper Baldry et al. (1998c) in collaboration with Don Kurtz and Tim Bedding. I observed and reduced the spectroscopic data with the supervision of T. Bedding. D. Kurtz provided the analysis of the photometric data taken at the same time as the spectroscopic data. This chapter is a rewritten and extended version of the paper.

7.1 Introduction

The roAp stars pulsate in high-overtone non-radial p-modes. The oscillation spectra of many of these stars reveal frequency multiplets – usually triplets – with equal frequency separations of the components. The separations are equal to, or very nearly equal to, the rotation frequency (determined from the variation of spectrum and light as the star rotates).

One explanation of the observed triplets is that a set of rotationally perturbed m-modes is excited, e.g. $\ell = 1$ dipole modes with $m = -1$, 0, +1. The observed frequencies can be written as (Ledoux 1951)

$$\nu_m = \nu_0 - m(1 - C_{n\ell})\nu_{rot} \tag{7.1}$$

where $C_{n\ell}$ is a constant that depends on the structure of the star. For A-star models with the expected pulsation modes for roAp stars, Takata & Shibahashi (1995) found $C_{n\ell} \approx 0.003$–0.010. However, in the best-observed roAp star HR 3831, Kurtz et al. (1992) were able to show that $C_{n\ell} < 2 \times 10^{-5}$. This is two orders of magnitude less than the theoretically predicted values, and suggests that the frequency splitting is precisely the rotational frequency.

Another explanation for a frequency multiplet is that it is produced by a single pulsation mode (e.g., $\ell = 1$, $m = 0$) whose amplitude is modulated[1] by rotation. This naturally produces a frequency splitting that is precisely equal to the rotation frequency. In some roAp stars, the amplitude of the pulsation has been observed to modulate with rotation

[1] In this chapter, we use the verb *to modulate* and its derivatives to describe changes in amplitudes and phases with rotation, and the verb *to vary* for other types of changes.

in phase with the magnetic variation. To explain this phenomena, the oblique pulsator model was proposed by Kurtz (1982), and has been extensively developed by Shibahashi & Takata (1993; Takata & Shibahashi 1994, 1995). In this model, the magnetic and pulsation axes are aligned but are oblique to the rotation axis. The observed amplitude modulation is then due to the variation in the angle between the pulsation axis and the line of sight as the star rotates.

In an alternative model, the spotted pulsator model (Mathys 1985), the pulsation and rotation axes are aligned (or there are radial $\ell = 0$ modes), but the ratio of flux to radius variations varies over the surface because of differences in the flux and temperature caused by spots associated with the magnetic field. The observed radial velocity (RV) amplitude is then constant, but the photometric amplitude modulates as the star rotates. Therefore, the two models can be distinguished by RV observations. Matthews et al. (1988) found RV amplitude variation in HR 1217 which favoured the oblique pulsator model, but this star is multi-periodic, so the observed variation could have been caused by beating among pulsation frequencies. Kurtz et al. (1994a) proposed that the two models could easily be distinguished by RV measurements of HR 3831. This roAp star has one dominant pulsation mode with a period of 11.7 min, has a large photometric amplitude modulation including a phase reversal (Kurtz et al. 1994a, 1997) and is bright enough for accurate RV measurements ($V = 6.25$).

In this chapter, we look at RV changes and Hα profile changes in HR 3831. We find that the radial velocities are modulated with the rotation of the star. A frequency analysis of the Hα RV shows a frequency triplet with the same spacing and amplitude ratios as in contemporaneous photometric observations which we obtained at the South African Astronomical Observatory. This is expected in the oblique pulsator model, and in clear disagreement with the prediction of the spotted pulsator model.

We also studied this star using some of the other techniques that were used in Chapters 5–6. These include cross-correlations of different wavelength regions, line-shifts of the Hα bisector and intensity measurements across the Hα line. While the oblique pulsator explains most of the observed rotational modulations, aspects of the spotted pulsator model and perturbed m-modes may also have an influence on the pulsations in this star.

7.1.1 Basic data for HR 3831

HR 3831 (IM Vel, HD 83368, HIP 47145) has a binary companion with $V = 9.09$ with a separation of 3.29 arcsec. The brightness of HR 3831 is often quoted as $V = 6.17$ which is from the combined flux measurement (see Kurtz et al. 1994a). The parallax has been measured by the *Hipparcos* mission (ESA 1997) to give a distance of 72.5 ± 4 pc to the star. Using $V = 6.25$, this distance, an effective temperature of 8000 ± 200 K (Kurtz et al. 1994a) and a bolometric correction of -0.13 (Schmidt-Kaler 1982), we obtain $L = 13.4 \pm 1.5 L_\odot$ and $R = 1.9 \pm 0.2 R_\odot$.

The oscillation spectrum of HR 3831 has a well-known frequency septuplet around 1428 μHz, plus frequency multiplets at the harmonics (Kurtz et al. 1997). However, there are just four frequencies which have photometric (Johnson B) amplitudes above 0.3 mmag and that are detectable in our data. These include a triplet around the princi-

pal mode ($\nu_{-1} = 1423.95\,\mu$Hz, $\nu_0 = 1428.01\,\mu$Hz, $\nu_{+1} = 1432.07\,\mu$Hz) and the first harmonic ($2\nu_0 = 2856.02\,\mu$Hz). The splitting of the triplet is the rotation frequency ($\nu_{\rm rot} = 4.06\,\mu$Hz) giving $P_{\rm rot} = 2.851976$ d, under the assumption that the oblique pulsator model is correct. Unlike the triplet in α Cir, where the amplitudes of the two sidelobes are about 10 percent of the principal amplitude, the amplitudes of ν_{-1} and ν_{+1} are larger than the amplitude of the central frequency. This means, that during the rotation cycle of HR 3831, the amplitude measured at ν_0 goes through two maxima with two phase reversals. In terms of the oblique pulsator model, the star pulsates in an $\ell = 1$ dipole mode which is sufficiently oblique to the rotation axis that as the star rotates we see first one pole and then the other.

Kurtz et al. (1990; Kurtz 1990) describe a generalised oblique pulsator model in which the effects of both the magnetic field and rotation were taken into account (see also Dziembowski & Goode 1985, 1986). In this model, the perturbation to the star's eigenfrequencies by the magnetic field dominates, leading to the conclusion that the pulsation axis is locked to the magnetic axis. Two parameters related to the amplitude ratios in the frequency triplet were defined:

$$P_1 = \frac{A_{+1} + A_{-1}}{A_0} = \tan i \tan \beta \,, \tag{7.2}$$

where i is the inclination of the rotation axis to the line of sight, and β is the angle between the rotation axis and the pulsation axis; and

$$P_2 = \frac{A_{+1} - A_{-1}}{A_{+1} + A_{-1}} = \frac{C_{n\ell}\,\nu_{rot}}{\nu_1^{(1)mag} - \nu_0^{(1)mag}} \,, \tag{7.3}$$

where the perturbation to the eigenfrequencies (by the magnetic field) depends on $|m|$ such that $\nu = \nu^{(0)} + \nu_{|m|}^{(1)mag}$. From the photometric results for HR 3831 covering 1993 to 1996 (Kurtz et al. 1997), $P_1 = 8.6 \pm 0.2$ and $P_2 = -0.097 \pm 0.004$.

7.2 Observations

7.2.1 Spectroscopy

We have obtained intermediate-resolution spectra of HR 3831 using the coudé spectrograph (dispersion of 0.49 Å/pixel) on the 74-inch Telescope at Mt. Stromlo, Australia. We have a total of 1400 spectra from a one week period in 1997 March (Table 7.1), with each spectrum having a minimum of 60 000 photons/Å. The average number of photons/Å in each spectrum was 270 000. The exposure time was 100 seconds, with an over-head between exposures of 20 seconds.

All of the CCD images were reduced to spectra using the same procedures that were used on the Stromlo data in Chapter 5. Several observables were defined from the spectrum (velocities, intensities, bisector measurements), to produce a time series of measurements for each observable. For use in various measurements, a template spectrum was defined from 25 high-quality spectra (Figures B.1–B.2).

Table 7.1 Log of the spectroscopic observations of HR 3831

UT-date	No. of hours	No. of spectra	Julian dates $-2\,450\,000$
1997 Mar 10	1.37	26	517.88 – 517.94
1997 Mar 10	3.61	38	518.12 – 518.27
1997 Mar 11	10.03	203	518.88 – 519.29
1997 Mar 12	9.59	285	519.88 – 520.28
1997 Mar 13	2.22	59	520.88 – 520.97
1997 Mar 13	1.10	33	521.27 – 521.32
1997 Mar 14	10.57	319	521.87 – 522.31
1997 Mar 15	10.40	262	522.88 – 523.31
1997 Mar 16	9.40	158	523.87 – 524.27
1997 Mar 17	0.53	17	524.87 – 524.90

Table 7.2 Photometric (Johnson B) amplitudes and phases of the frequency triplet

frequency (μHz)	amplitude (mmag)	phase[a] (radians)	P_1	P_2
1423.95	1.91 ± 0.05	1.00 ± 0.03		
1428.01	0.52 ± 0.05	-1.16 ± 0.10	6.9 ± 0.7	-0.07 ± 0.02
1432.07	1.66 ± 0.05	1.03 ± 0.03		

[a] The phases are shifted compared to the those given in Baldry et al. (1998c) due to a different phase reference point (see Section 7.3).

7.2.2 Photometry

For the last five years, astronomers at the South African Astronomical Observatory (SAAO) and the University of Cape Town (UCT) have been monitoring the oscillations in HR 3831 using high-speed photometry (Kurtz et al. 1997). We have selected a subset of their data which is centred on the time of our spectroscopic observations. These data were obtained on 26 nights (one hour of high-speed photometry per night) spanning the dates JD 2 450 402 to 2 450 618.

The photometry was analysed to find the amplitudes and phases of the frequency triplet (see Table 7.2) in order to compare with our spectroscopic results. The amplitudes of the triplet are within 2σ of the amplitudes from Kurtz et al. (1997). For further details, in particular showing the pulsation amplitude and phase as a function of rotation phase, see Baldry et al. (1998c).

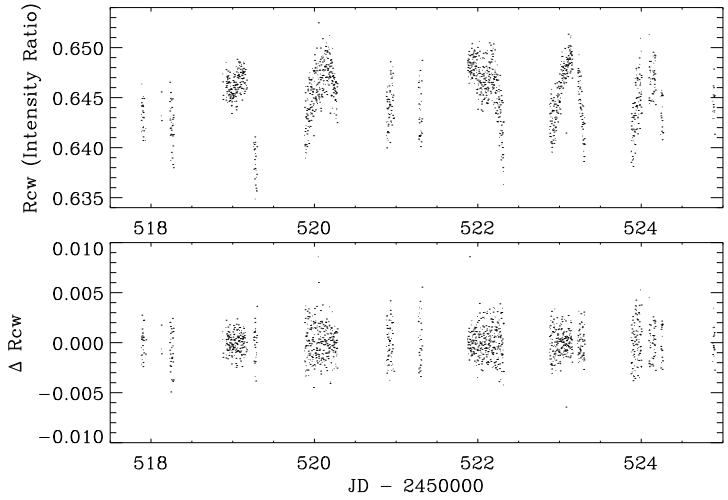

Figure 7.1 R_{cw} time series before and after high-pass filtering

7.3 Time-series analysis

To illustrate the various methods of analysing the time series for each spectroscopic observable, we look at an observable which has a high signal-to-noise ratio in the oscillation spectrum. This observable, called R_{cw}, is a ratio of the Hα core to wing intensity. In particular, we measured the intensity in a filter with FWHM~ 4Å divided by a filter with FWHM~ 31Å. This is similar to the R_{cw} measurements used in Chapter 6 and Baldry et al. (1998c) but using slightly narrower filters.

Each time series from the spectroscopic measurements was high-passed filtered and a few outlying points were removed. The R_{cw} time series before and after high-pass filtering is shown in Figure 7.1. There is a variation in the raw data of about 1 percent during the night. This is possibly due to varying contamination of the HR 3831 spectrum from its binary companion. As the pair of stars rotate in the coudé focal plane, there will be less contamination when the stars line up perpendicular to the slit and more contamination when the stars line up along the slit. Alternatively, the variation could be due to instrumental effects that are a function of elevation of the telescope. In either case, the change in the measured oscillation amplitude will be of the order of 1 percent over the night. This is not significant for our results, especially since there is no obvious systematic effect as a function of the rotation phase of HR 3831.

Next, a simultaneous fit of the frequency triplet and the first harmonic was made to the high-pass filtered data, using a weighted least-squares fitting routine. The amplitudes and phases were fitted, using the well-known frequencies (see Section 7.1.1), by the function $A\sin(2\pi\nu(t-t_0)+\phi)$ where $t_0 =$ JD 2 450 522.51746. Our phase reference point t_0 is equal to the reference point of Kurtz et al. (1997) plus 775 times $P_{\rm rot}$. This maintains the same relationship between the phases of the frequency triplet. The fit of the frequency triplet to the R_{cw} data is shown in Table 7.3 (the results for three sets of filters are shown).

Table 7.3 R_{cw} amplitudes and phases of the frequency triplet in HR 3831. The observable R_{cw} is the ratio between the mean intensity in a narrow filter with FWHM $F1$ and in a filter with FWHM $F2$ centred on Hα. For the three observables in this table, the average values are about 0.65 (see Figure 7.1 for the raw data in the second case).

$F1$ (Å)	$F2$ (Å)	frequency (μHz)	amplitude (ppm)	phase (radians)	P_1	P_2
2.9	23.5	1423.95	1340 ± 46	-0.82 ± 0.03	15.8 ± 4.7	$+0.02 \pm 0.02$
		1428.01	172 ± 45	-1.28 ± 0.27		
		1432.07	1386 ± 46	-0.78 ± 0.03		
3.9	31.4	1423.95	1334 ± 41	-0.71 ± 0.03	14.0 ± 3.5	-0.08 ± 0.02
		1428.01	177 ± 40	-1.58 ± 0.23		
		1432.07	1139 ± 41	-0.78 ± 0.04		
5.9[a]	45.1[a]	1423.95	1107 ± 41	-0.64 ± 0.04	12.4 ± 3.4	-0.10 ± 0.03
		1428.01	163 ± 41	-1.70 ± 0.25		
		1432.07	913 ± 41	-0.78 ± 0.05		

[a] This set of R_{cw} results uses the same filters as the R_{cw} results published in Baldry et al. (1998c). The results are slightly different due to a different weighting in the least-squares fitting routine, and there is also a change in phase reference point.

The R_{cw} oscillation amplitude spectrum is shown in Figures 7.2–7.3. Figure 7.3 shows that the frequency triplet is resolved, but with some aliasing or power shifting between the frequencies as can be seen from the spectral window. The amplitude of the spectral window at $\pm\nu_{rot}$ and at $\pm 2\nu_{rot}$ is about 20 percent. Also, the simultaneous fit gives amplitudes in ppm of 1330, 180 and 1140 for the triplet, whereas the amplitudes in the oscillation spectrum are 1100, 560 and 890 (note that ratio between A_{+1} and A_{-1} is about the same).

Another way to consider the aliasing is that the data have incomplete and biased sampling of the rotation phase of HR 3831. A good diagnostic of the data, and better for interpretation assuming that there is one mode that is amplitude modulated, is to plot the amplitude and phase of the pulsation (at ν_0) as a function of rotation phase. The data were divided into 20 separate time periods between 0.5 and 3.6 hours long and including between 17 and 107 spectra. For each time period, the amplitude and phase were measured at 1428.01 μHz. The R_{cw} results are shown in Figure 7.4. The two lines represent different fits to the data:

(i) The dashed line represents a modulation using the amplitudes and phases of the R_{cw} frequency triplet (from Table 7.3), which are from a six parameter fit to the complete time series. In other words, it shows the beating effect of the three close frequencies (ν_{-1}, ν_0, ν_{+1}). The good agreement between the modulation in amplitude and phase from the separate time periods and the modulation from the frequency triplet supports the accuracy of the simultaneous fit to the triplet.

(ii) The dotted line represents a fit which is obtained by scaling and phase shifting from

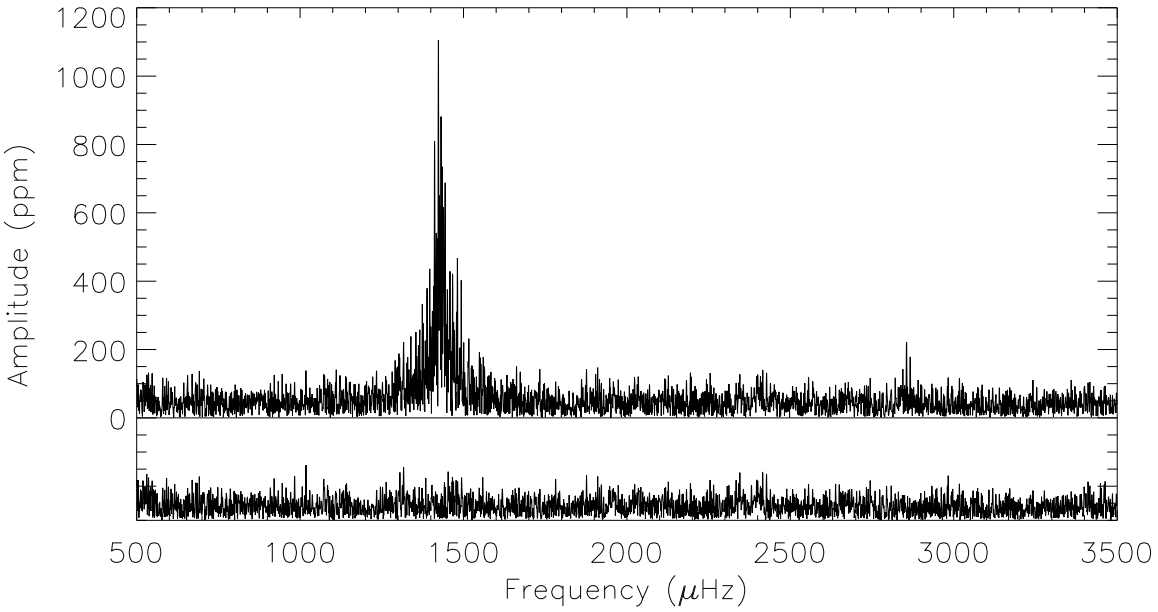

Figure 7.2 R_{cw} amplitude spectrum. The lower panel is the pre-whitened amplitude spectrum after subtracting a simultaneous fit of the frequency triplet and the harmonic.

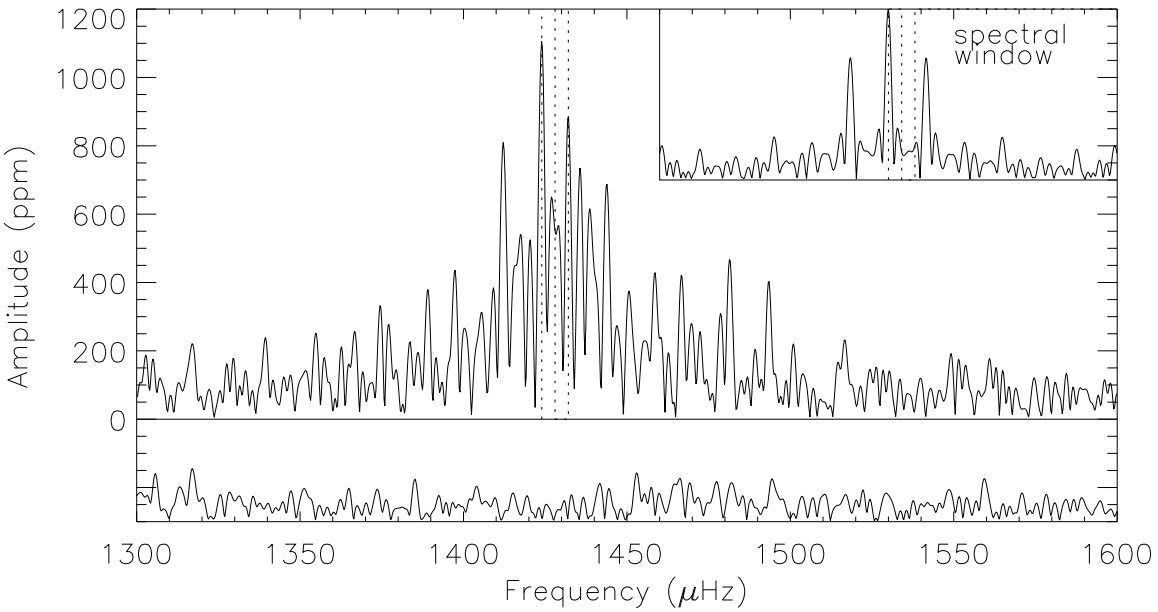

Figure 7.3 Close-up of Figure 7.2, with the dotted lines showing the frequencies of the triplet. The inset shows the amplitude spectrum of the window function on the same frequency scale, with the dotted lines having the same spacing as in the triplet.

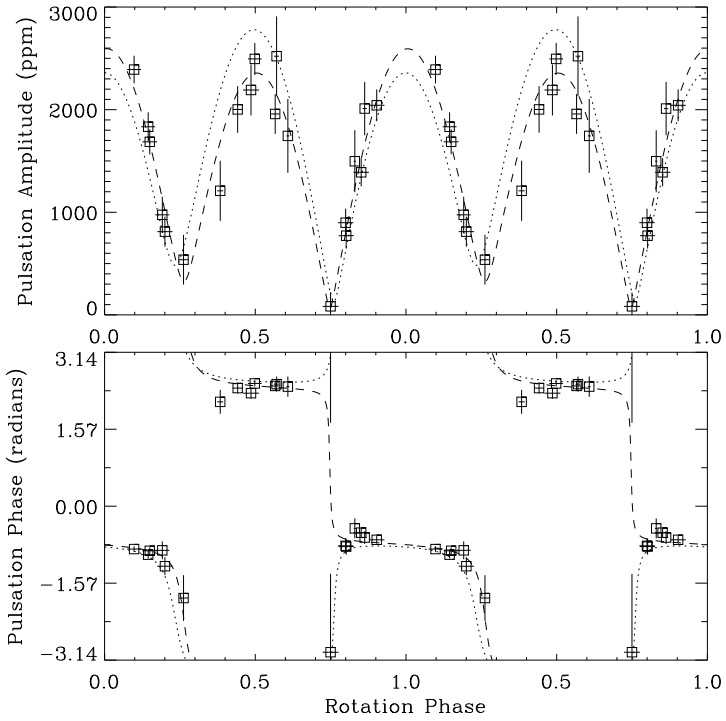

Figure 7.4 R_{cw} amplitude and phase of the central frequency as a function of rotation phase. The squares represent the data divided into 20 separate time periods between 0.5 and 3.6 hours long. The vertical lines are error bars, while the horizontal lines show the length of the time period. The dashed line represents a fit based on the measurement of the frequency triplet from the complete time series, and the dotted line represents a fit which is scaled and phase shifted from the photometric frequency triplet. Note that the data are plotted twice.

the photometric analysis of the triplet (from Table 7.2), in effect, a two parameter fit to the amplitudes and phases of the separate time periods. The shape of the amplitude and phase modulation is the same as the beating effect of the photometric triplet, while one parameter is the scaling of the amplitude and the other parameter is the shift of the pulsation phase. In this case, a reasonable fit is obtained to the R_{cw} data.

In conclusion, we have clearly detected the triplet in the equivalent-width of Hα (using R_{cw}) with the amplitudes of the three components in about the same ratio as seen in photometry. The R_{cw} measurement, as in α Cir, provides a high signal-to-noise spectral measurement of the pulsation.

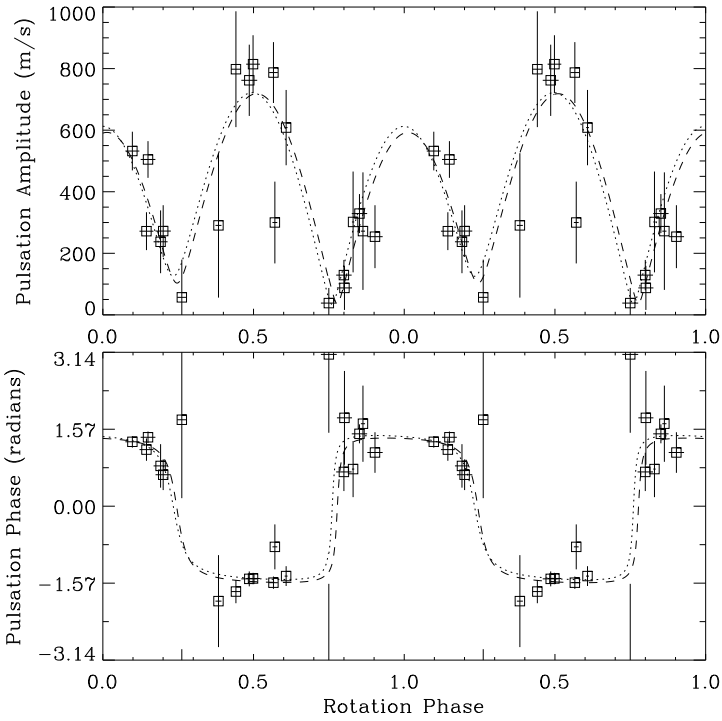

Figure 7.5 Hα velocity amplitude and phase of the central frequency as a function of rotation phase (band no. 87). The dashed line represents a fit based on the measurement of the frequency triplet from the complete time series, and the dotted line represents a fit scaled and phase shifted from the photometric frequency triplet. There is excellent agreement between the two fits, which supports the oblique pulsator model and rules out the spotted pulsator model.

7.4 Velocities of different wavelength bands

In this section, we look at the velocity amplitude and phase of different wavelength bands using a cross-correlation technique. The reduction method is the same as that used on α Cir (see Section 5.3.2), with a telluric band used as a velocity fiducial (Section 5.3.3). The spectrum of HR 3831 was divided into 90 bands, most having the same wavelength range as shown in Tables 5.3–5.4, the difference being that the spectrum of HR 3831 was taken from 6100Å to 7100Å, which is 100Å higher than the range used in the α Cir analysis. The results for 10 selected bands are shown in Table 7.4.

7.4.1 Hα velocity

First, we look at the Hα velocity as measured using the cross-correlation of band no. 87. This band should not be significantly affected by blending and has good signal-to-noise. The Hα velocity amplitude and phase as a function of rotation phase are shown in Figure 7.5. There is excellent agreement between the fit based on the measurement of the frequency triplet (Table 7.4) and the fit scaled and phase shifted from the photometric data

Table 7.4 Velocity amplitude and phases for selected wavelength bands using a cross-correlation technique. The bands selected were those having a combined signal-to-noise[a] ratio of greater than 9 for the frequency triplet, except only one band across the Hα line is included (band no. 87). A telluric band from 6864 to 6881Å is used as a velocity reference (band no. 80).

band[b] range (Å)	frequency (μHz)	amplitude ($m\,s^{-1}$)	phase (radians)	P_1[c]	P_2	Fig.
no. 13	1423.95	377 ± 51	0.82 ± 0.13			
	1428.01	92 ± 50	-0.67 ± 0.57	—	-0.18 ± 0.12	B.3
6140.6–6150.9	1432.07	260 ± 51	0.89 ± 0.20			
no. 14	1423.95	524 ± 61	2.45 ± 0.12			
	1428.01	26 ± 61	—	—	-0.32 ± 0.12	B.4
6152.9–6164.6	1432.07	273 ± 61	2.41 ± 0.23			
no. 18	1423.95	1108 ± 69	0.07 ± 0.06			
	1428.01	228 ± 68	-1.33 ± 0.30	6.6 ± 2.3	-0.48 ± 0.07	7.8
6194.0–6197.5	1432.07	392 ± 69	0.09 ± 0.18			
no. 33	1423.95	1140 ± 62	0.54 ± 0.05			
	1428.01	222 ± 62	-0.96 ± 0.28	7.6 ± 2.4	-0.34 ± 0.05	B.5
6325.8–6333.2	1432.07	556 ± 62	0.46 ± 0.11			
no. 42	1423.95	600 ± 64	1.26 ± 0.11			
	1428.01	118 ± 64	-0.77 ± 0.57	—	-0.13 ± 0.09	B.6
6414.0–6422.9	1432.07	458 ± 64	0.70 ± 0.14			
no. 54	1423.95	348 ± 60	1.64 ± 0.17			
	1428.01	88 ± 60	-0.44 ± 0.75	—	$+0.10 \pm 0.11$	B.8
6521.8–6528.2	1432.07	423 ± 60	1.62 ± 0.14			
no. 58	1423.95	1378 ± 132	2.36 ± 0.10			
	1428.01	131 ± 131	-0.47 ± 1.49	—	-0.60 ± 0.13	B.9
6596.3–6607.1	1432.07	346 ± 132	2.83 ± 0.39			
no. 81[d]	1423.95	63 ± 12	-2.59 ± 0.19			
	1428.01	16 ± 12	1.99 ± 0.80	—	$+0.03 \pm 0.13$	B.10
6881.5–6901.6	1432.07	68 ± 12	2.54 ± 0.18			
no. 87[e]	1423.95	343 ± 22	1.58 ± 0.06			
	1428.01	94 ± 22	-0.81 ± 0.24	6.9 ± 1.8	-0.05 ± 0.05	7.5
6545.4–6578.2	1432.07	309 ± 22	1.42 ± 0.07			
no. 90[f]	1423.95	743 ± 87	0.95 ± 0.12			
	1428.01	116 ± 87	-1.15 ± 0.84	—	-0.35 ± 0.12	B.12
7070.2–7079.5	1432.07	357 ± 87	1.28 ± 0.25			

[a] The rms-noise is about 1.38 times the formal 1σ error on the amplitude measurements.
[b] The band number relates to the bands used in Chapter 5.
[c] Only the bands where the central amplitude is higher than 2σ are included. For the other bands, the error in this parameter is large and significantly non-gaussian.
[d] This band contains a significant number of telluric lines, see discussion in Section 5.5.1.
[e] This band represents the velocity of the Hα line. These results are different to those published in Baldry et al. (1998c) because the band is wider and the telluric band used as a reference is different.
[f] This is a new band not included in Chapter 5.

(Table 7.2). This supports the oblique pulsator model and rules out the spotted pulsator model. In the latter model, the pulsation velocity amplitude and phase should be constant during the rotation of the star, which is clearly not the case.

The excellent agreement between the Hα velocity and photometry, in terms of the relative modulation as a function of rotation phase, is reflected in the fact that the parameters P_1 and P_2 are nearly the same between the two time series (compare Table 7.2 with band 87 from Table 7.4). Within the oblique pulsator model, these parameters are expected to be the same for different observables (see Section 7.1.1). If the frequency triplet were caused by three different modes, then the ratios between the amplitudes of the modes (quantified by P_1 and P_2) would be expected to vary depending on the observable. Therefore, this agreement between the Hα velocity and photometry argues in favour of the oblique pulsator model rather than for different modes. However, this is a weak argument because the amplitude ratios could be nearly the same even in the case of different modes. The main arguments against different modes come from the years of photometric analysis of HR 3831 (e.g, Kurtz et al. 1990, 1993, 1994a, 1997): (i) the frequency splitting is exactly or nearly exactly the rotation frequency (see Section 7.1), and (ii) the ratios between the amplitudes of the frequency triplet has remained nearly constant over time. For these reasons, it is considered unlikely that the observed frequency triplet in HR 3831 is caused by different modes, in particular rotationally perturbed m-modes.

In Baldry et al. (1998c), we noted a possible rotational phase lag between the radial velocity (RV) amplitude maximum and the photometric amplitude maximum, of about 0.06 rotation cycles. However, from the results shown in Figure 7.5, the RV maximum and photometric maximum are within 0.02 rotation cycles of each other. The change from the earlier results arises from the use of a different telluric reference wavelength region. In Baldry et al. (1998c), a large region from 6865 to 6931Å was used, which included band nos. 80, 81 and 82, in order to maximise the signal-to-noise ratio. In this chapter, we find a significant signal arising from the wavelength region of band 81 (see Table 7.4) and this is likely to be the cause of the phase lag noted in Baldry et al. (1998c). Band 80 is used as the telluric reference band in this chapter. The justification for using this band is that it has the lowest percentage (about 2%) of absorption that is attributable to lines from the star (see discussion in Section 5.5.1). To summarise, the Hα RV amplitude is better represented by the results in this chapter, whereas the results in Baldry et al. (1998c) are slightly contaminated by metal lines around band 81.

7.4.2 Metal lines

The velocity amplitude and phase in HR 3831 varied significantly between different wavelength bands, as was seen in α Cir (Chapter 5). Figures 7.6–7.7 show the amplitude versus phase for the 26 metal bands with the highest signal-to-noise ratios (plus one band across Hα) in HR 3831. The results measured at the frequencies ν_{-1} and ν_{+1} are plotted separately, while the amplitude and phase of ν_0 are not plotted because the signal-to-noise ratio is significantly lower at this frequency. There are two aspects to the results which we will consider: the modulation of the measured pulsation with rotation and the variation of the amplitude and phase between different wavelength bands. The first is characterised

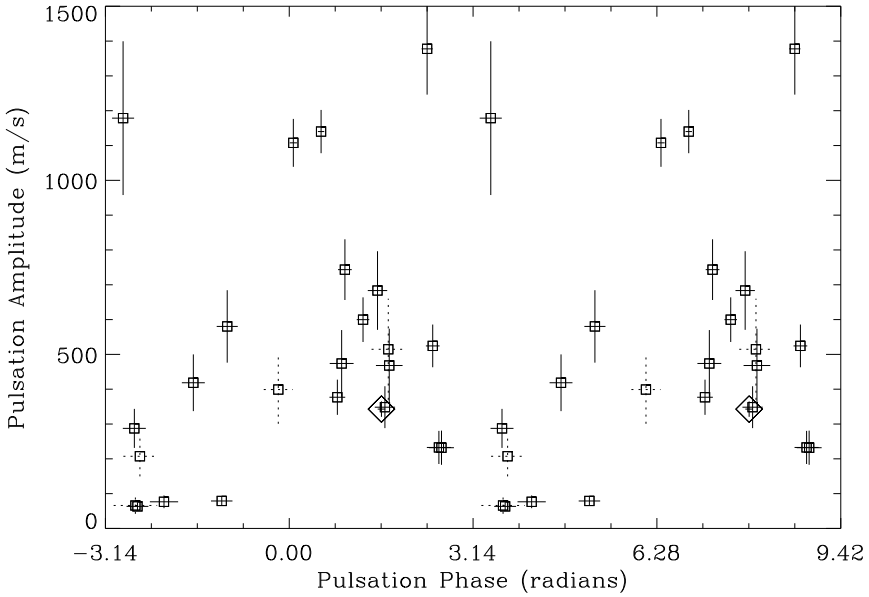

Figure 7.6 Velocity amplitudes and phases measured at the frequency ν_{-1} in HR 3831 for different wavelength bands. Bands with S/N greater than 3 are plotted with solid lines, those with lower S/N use dotted lines. The same 27 bands are plotted in Fig. 7.7, chosen so that the *combined* S/N is greater than 5. Only one band across Hα is included, which is shown using a diamond. Note that the data are plotted twice for clarity.

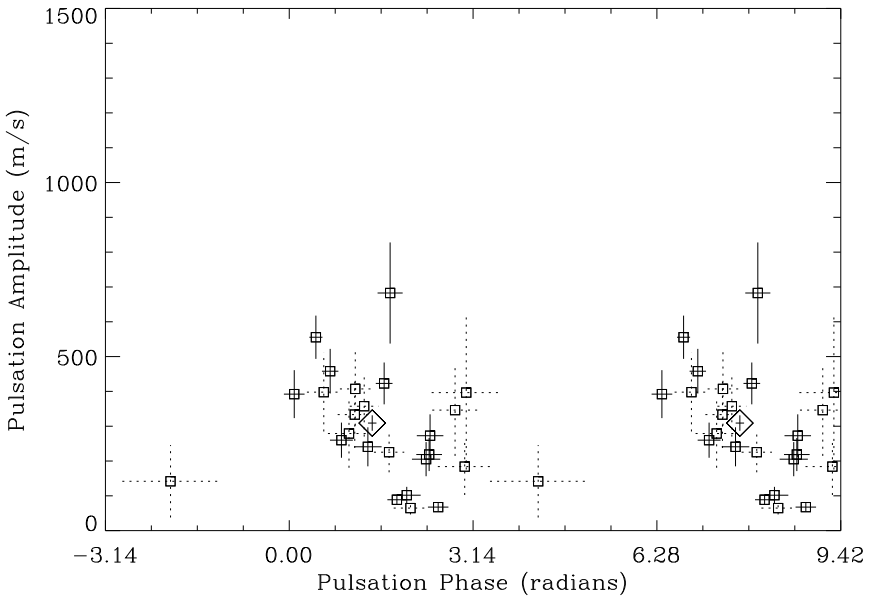

Figure 7.7 Same as Figure 7.6, but for the frequency ν_{+1}.

by the difference in amplitude and phase between ν_{-1} and ν_{+1}.

Rotational modulation

There is a significant difference between the results for ν_{-1} (Fig. 7.6) and ν_{+1} (Fig. 7.7). Firstly, the amplitudes vary between 0 and 1500 m s^{-1} for ν_{-1}, whereas the amplitudes for ν_{+1} are all below 800 m s^{-1}. Secondly, the phases range across 2π for ν_{-1}, while the phases for ν_{+1} range between 0 and π except for one low S/N band. This is not as expected from the oblique pulsator model. In this model, for each band, the phase of ν_{-1} and ν_{+1} should be the same and the amplitudes should be nearly the same ($A_{+1} \approx 0.87 \times A_{-1}$ from Table 7.2). Therefore, these results suggest that the two frequencies measured are separate modes, rather than rotational 'side lobes' of one principal mode. However, there is strong evidence for the oblique pulsator model as described in Section 7.4.1. Therefore, we need to consider another explanation within the framework of the oblique pulsator model. We first look at some selected bands, in terms of their modulation of amplitude and phase with rotation.

Recall that the oblique pulsator model involves parameters P_1 and P_2 (Eqs. 7.2 & 7.3). All the measured spectroscopic observables in this chapter produce values for P_1 that are within 3σ of the photometric value. There are large errors in this parameter because it depends critically on the amplitude measured at ν_0, which is typically less than two or three times the noise level in our data. The parameter P_2 does vary significantly between different observables. It can be measured with higher accuracy since it does not depend on the small central amplitude. From the measured velocity amplitudes, there are three spectral bands (18, 33 and 58) that have values of P_2 that are formally 4–5σ different from the photometric value (see Table 7.4). To test whether this is a significant change or just a product of aliasing, we looked at the modulation in velocity amplitude and phase as a function of rotation phase. Figure 7.8 shows this modulation for band 18. While the amplitude modulation could be fitted reasonably well by scaling from the photometry, the discrepancy is obvious with the phase modulation. There is a noticeable pulsation phase change from rotation phase 0.8 through 1.0 to 0.2, while the photometric phase is nearly constant. Similar effects are evident from bands 33 and 58 (see Figures B.5 and B.9).

As well as the parameters P_1 and P_2, which relate the amplitudes of the frequency triplet, there are also phase differences between the frequencies. For many bands, there is significant difference between the phases measured at ν_{+1} and ν_{-1}. In our measurements, the equality of phase ϕ_{+1} and ϕ_{-1} means that the amplitude maxima occur at rotation phases 0.0 and 0.5 with phase jumps in between. Therefore, any phase difference $\phi_{+1} - \phi_{-1}$ implies that there is a shift of the amplitude maxima. For example, there is a small shift in the amplitude maxima of band 42 (Figure B.6) and larger shifts, but with low signal-to-noise, of bands 48 and 82 (Figures B.7 and B.11).

These results are not sufficient evidence to discard the oblique pulsator model, because they could be explained by variations in the ratios between the metal lines in the bands, due to spots, as the star rotates. Alternatively, there is a possibility that there is an actual change in the pulsation phase and amplitude (as opposed to a pseudo-change caused by a variation in blending) associated with spots on the star. So while the spotted pulsator

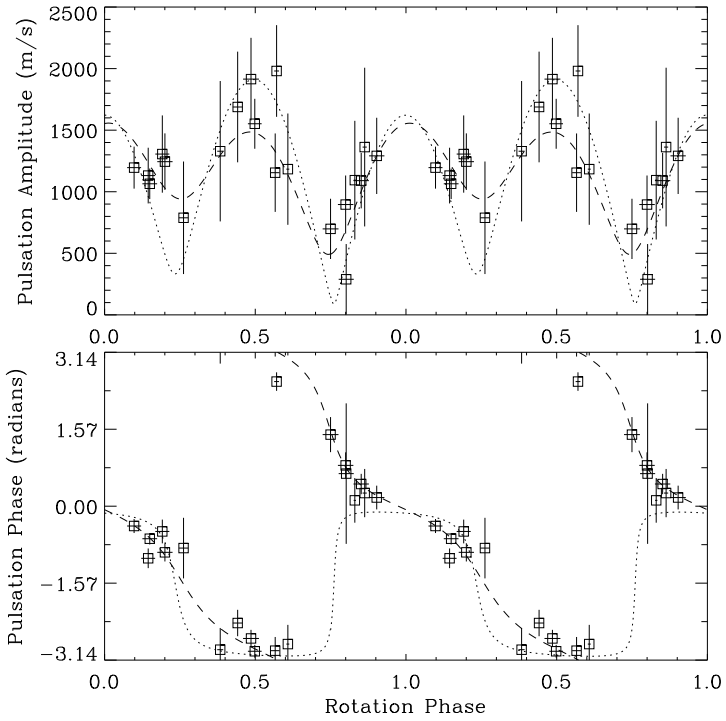

Figure 7.8 Velocity amplitude and phase of band no. 18 as a function of rotation phase. The dashed line represents a fit based on the measurement of the frequency triplet from the complete time series, and the dotted line represents a fit scaled and phase shifted from the photometric frequency triplet.

model is ruled out in its original form, spots may be having an influence on the pulsation.

Amplitude and phase variations between bands

In Chapter 5, it was suggested that the amplitude and phase variations between wavelength bands in α Cir could be explained by a radial node in the atmosphere. We see amplitude and phase variations in HR 3831 that are somewhat similar in the case of ν_{-1} (Fig. 7.6), and with smaller but still significant variations in the case of ν_{+1} (Fig. 7.7). However, there is no obvious division between two sets of bands that are pulsating in anti-phase with each other, as was seen in α Cir (Figure 5.8). If these HR 3831 results represent true velocity amplitudes and phases at various depths in the atmosphere, then an explanation that includes running waves is necessary. Alternative explanations could involve spots on the surface or blending, which causes the measured phase to deviate from the true velocity phase.

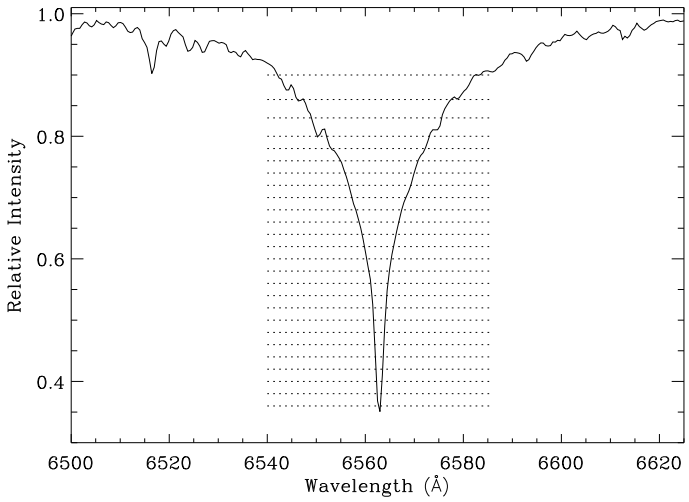

Figure 7.9 The Hα line in HR 3831. The dotted lines divide the 25 contiguous sections used in the bisector velocity and width analysis (Section 7.5).

7.5 Hα profile variations

The Hα line in each spectrum was divided into 25 contiguous horizontal sections, between relative intensities 0.35 and 0.9 (Figure 7.9). For each section, a bisector velocity (average position of the two sides) and a width were calculated. For the velocity measurements, a telluric band (no. 80) was used as a fiducial.

7.5.1 Bisector velocities

The velocity amplitude and phase of the pulsation as a function of relative intensity in the Hα line are shown in Figure 7.10, with measurements at frequencies ν_{-1} and ν_{+1}. The amplitudes and phases are in good agreement between the two frequencies, which means that the shape of the rotational modulation is similar for each velocity measurement. Figure B.13 shows the rotational modulation from the velocity at a height of 0.40. It is similar to the modulation from the cross-correlation velocity of Hα (Figure 7.5), but with about twice the amplitude. This is expected because the cross-correlation velocity is a weighted average of the bisector velocities and the velocity amplitude at 0.40 is higher than average.

The variation in amplitude and phase as a function of relative intensity (Fig. 7.10) is similar to that seen in α Cir (Fig. 6.2), particularly the drop in amplitude between heights 0.4 and 0.6 (a comparison is shown in Figure 8.2). However, assuming that the bisector line-shift represents the velocity at different heights in the atmosphere, we expect to see less relative variation in the bisector velocity amplitude in HR 3831 than α Cir. This is because the separation between radial nodes in the atmosphere is larger in HR 3831 due to the fact that it pulsates at a lower frequency and that the two stars have similar

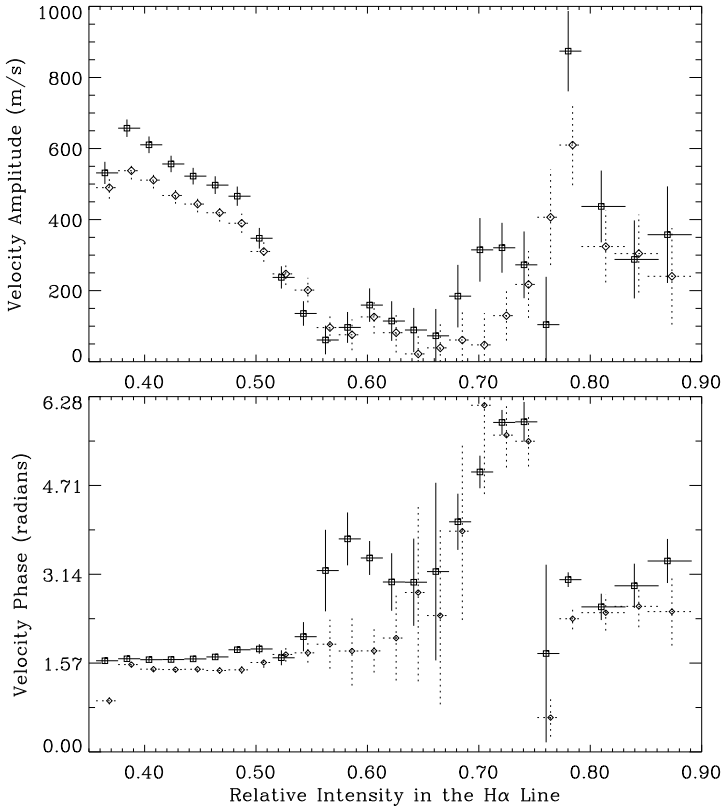

Figure 7.10 Amplitudes and phases of the pulsation for the bisector velocity at different heights in the Hα line. Squares with solid lines represent ν_{-1} and diamonds with dotted lines represent ν_{+1}. For each measurement, the vertical line is an error-bar while the horizontal line shows the extent of the section in the Hα line.

fundamental properties (see Sections 6.1.1 and 7.1.1). Two possible explanations are that: (i) the Hα line forming region in HR 3831 is more extended than in α Cir and coincidently the Hα bisector behaves in a similar way; (ii) the assumption that the bisector represents velocities at different heights is incorrect.

The variation in amplitude and phase is less similar to α Cir above a height of 0.7. For instance, there is a noticeable amplitude peak and phase reversal around 0.73 in the bisector of α Cir which is not evident in HR 3831. The bisector measurements above a height of 0.7 in α Cir are partially affected by blending (Section 6.3.2). Therefore, some of the differences in the bisector velocity results between the two stars are probably due to a difference in blending.

To summarise, there is no significant difference in the rotational modulation of the bisector velocity between various heights. For the measurements below a height of 0.7, the relative variation in amplitude and phase is very similar to that observed in α Cir, which is puzzling. At each height, the amplitudes at the two frequencies in HR 3831 are about twice the amplitude of the principal frequency in α Cir.

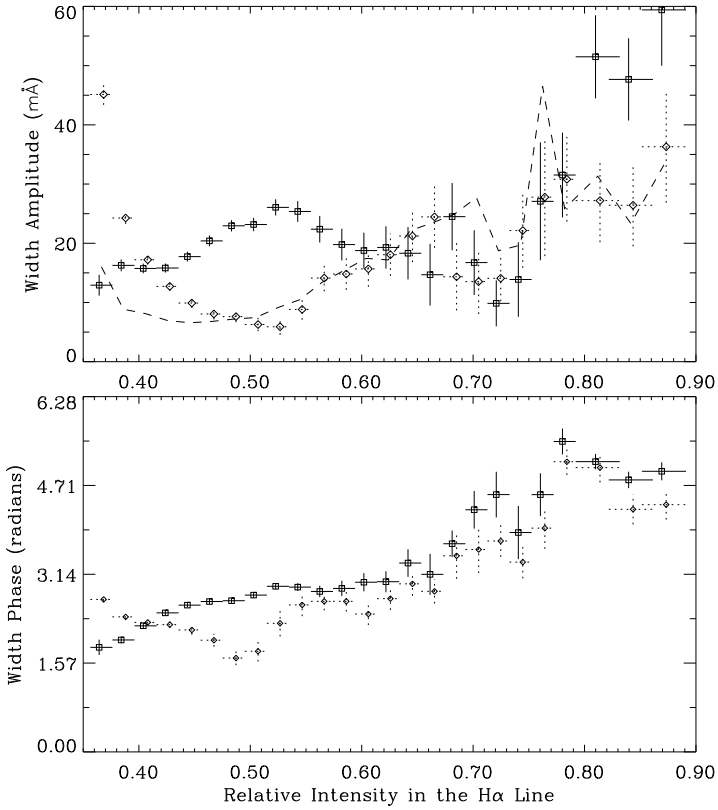

Figure 7.11 Amplitudes and phases of the pulsation for the width at different heights in the Hα line. Points with solid lines represent ν_{-1} and points with dotted lines represent the ν_{+1}. For each measurement, the vertical line is an error-bar while the horizontal line shows the extent of the section in the Hα line. The dashed line shows the effect on the width amplitude of an oscillation with an EW amplitude of 1000 ppm, with the profile variation described in Section 6.4.2. Note that 10 mÅ is equivalent to a dispersion of 457 m s^{-1} at Hα.

7.5.2 Widths

Changes in the width of the Hα line in HR 3831 at various heights are shown in Figure 7.11. The width amplitude and phase represent oscillations about a mean width, with measurements at two frequencies. These measurements are related to intensity and EW measurements, with the line resolved vertically rather than horizontally. The advantage of width measurements is that the width is naturally independent of the bisector velocity, i.e., the width is the difference in position between two sides of a line whereas the velocity is the average position. In order to compare with EW measurements, the dashed line shows the simulated width amplitudes for the profile variation described in Section 6.4.2 (see also Figure 6.6) with an EW amplitude of 1000 ppm (see Appendix A.3 for a width analysis of α Cir).

The most striking feature of Figure 7.11 is that there is such a difference in the measurements between the two frequencies. This means that, unlike for the bisector velocities,

the shape of the rotational modulation is varying between different heights. Three examples are shown to demonstrate the extremes (in terms of the parameter P_2) and the closest to the photometric modulation.

(i) Figure B.14 shows the modulation in width amplitude and phase at a height of 0.36. The pulsation width phase increases steadily during the rotation ($P_2 = 0.54 \pm 0.05$).

(ii) Figure B.15 shows the modulation at height 0.42. There is good agreement with the fit derived from the photometric triplet ($P_2 = -0.03 \pm 0.04$).

(iii) Figure B.16 shows the modulation at height 0.53. The width phase decreases steadily during the rotation ($P_2 = -0.63 \pm 0.07$).

To check the lowest measurement at height 0.36, which is sensitive to intensity changes in the core of the line, we took an intensity measurement using a filter with a full-width half-maximum of about 1Å. This measurement shows a similar rotational modulation with the parameter $P_2 = 0.33 \pm 0.03$ (Figure B.17). If we consider the two extremes, i.e., the width changes at heights 0.36 and 0.53: at rotation phases around 0.5 and 1.0 the width changes are in phase; whereas, at rotation phases around 0.25 and 0.75 they are in anti-phase. At both heights, the relative amplitude modulation (as defined by the dashed-line) is less than for other observables. Though we note that in the case of Figure B.14, the lowest data point deviates by 3–4σ deviation from the dashed-line.

If we look at Figure 7.11, the simple explanation is that we are seeing two modes that have different Hα profile variations. An alternative explanation — if HR 3831 is pulsating in an oblique mode — is that, as the star rotates, the profile variation modulates due to viewing different aspects of the same mode.

Chapter 8

RoAp stars: further discussion and conclusions

8.1 Velocity amplitudes and phases

8.1.1 Another case: γ Equ

Kanaan & Hatzes (1998) observed radial velocity variations in the roAp star γ Equ. Their observations consisted of high-resolution spectra in the range 5000–6000 Å, covering 3.5 h on 13 September 1994. There are four modes in the range 1330–1430 μHz (Martinez et al. 1996), which are unresolved in that data set. Kanaan & Hatzes fitted a sine curve of fixed frequency (1380 μHz), but variable amplitude and phase, to the velocity measurements of each individual line, effectively treating the modes as a single pulsation. They discovered that the velocity amplitude varied significantly from line to line (see Chapters 5 and 7 for similar results on α Cir and HR 3831).

We analysed some of these results on γ Equ from Table 1 of Kanaan & Hatzes (1998) in order to compare with the results on α Cir and HR 3831. From the table, which consisted of 70 metal lines, we took the amplitude A (m/s), σ_a (m/s) and the 'Time of Maximum' (JD). Note that the times of maximum quoted by Kanaan & Hatzes cover several pulsation cycles. We converted the times to phases using the pulsation period of 0.008387 d, and the phases were shifted so that a weighted mean was approximately zero. The phase error was taken to be the arcsin (σ_a/A). This phase error is in good agreement with the σ_b (days) quoted in their table for lines where A/σ_a is greater than 2. Fig. 8.1 shows amplitude versus phase for the 19 lines with the highest signal-to-noise ratio. The higher amplitude bands, plotted with solid lines, cover a range of 0.8 radians in pulsation phase (-0.26 to $+0.54$ in the figure). This is significantly less than the variation in phase seen in α Cir (Fig. 5.7) and HR 3831 (Fig. 7.6), where the bands cover virtually the whole range of phases (2π). Note that the rms-noise level in an oscillation spectrum is about $1.38\sigma_a$, therefore, $A/\sigma > 4$ is comparable to $A/\mathrm{noise} > 3$.

The difference between the results on γ Equ (Kanaan & Hatzes) and results on the other two roAp stars (this thesis), in terms of the variation in phase between different metal bands, could be due to: (i) wavelength region studied, 5000–6000 vs. 6000–7000,

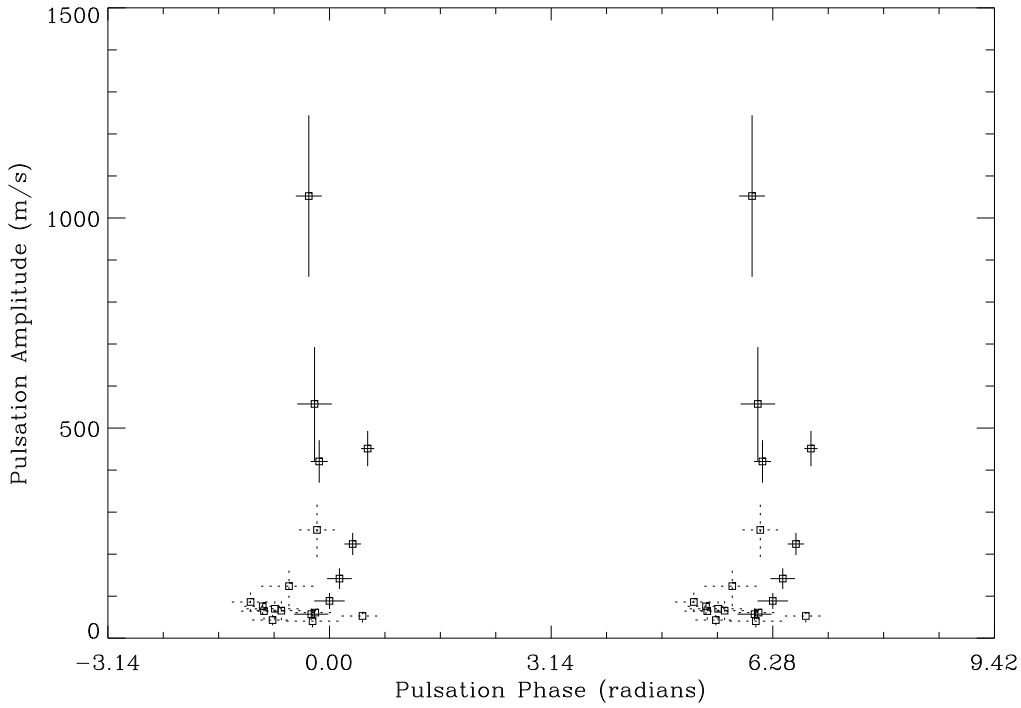

Figure 8.1 Amplitudes and phases of the pulsation in γ Equ for different metal lines, using results from Kanaan & Hatzes (1998). Lines with A/σ_a greater than 4 are plotted with solid lines, those with $2.5 < A/\sigma_a < 4$ are plotted with dotted lines. Note that the data are plotted twice for comparison with Figs. 5.7, 5.10, 7.6 and 7.7.

(ii) spectrograph resolution, 0.2Å vs. 1.5Å, (iii) pulsational characteristics of the star. Further high-resolution studies of these roAp stars will be able to distinguish among these causes.

8.1.2 Depth and surface effects

What are the causes of the velocity amplitude and phase variations, and of the Hα bisector variations?

The main hypothesis is that there is a significant change in pulsation amplitude and phase with geometric depth in the atmosphere of an roAp star, with a radial node of a standing wave situated in the observable atmosphere. Absorption lines are formed at different depths and therefore sample different parts of the standing wave. This can explain a complete range of observed amplitudes plus a phase reversal.

An alternative hypothesis for these variations is that the amplitude and phase of a non-radial pulsation mode will vary over the surface of a star, and that each spectroscopic observable is related to an integral over the surface. Therefore, if the integrals are sufficiently different between observables, the measured amplitude and phase may vary significantly. These variations could be related to limb-darkening and / or spots.

Neither hypothesis can fully explain the range of phases seen in α Cir and HR 3831. There may be blending effects that cause deviations from the true velocity phases on top of the atmospheric depth or surface effects. The argument for this is quite strong given that less phase variations are seen in the high-resolution results of γ Equ, but as pointed out above, there may be other causes. Blending can be considered as blurring the distinction between velocity and temperature changes in a star.

Surface effects would be a good explanation if roAp stars were pulsating in modes with $\ell \geq 3$ because, for these modes, there are several patches on the surface that have alternating phase. However, the frequency triplets in many roAp stars suggest that dipole modes are predominant ($\ell = 1$). For these modes, the measured velocity amplitude and phase is not expected to vary significantly between different observables (due to surface effects), e.g., for a dipole mode with an axis that is aligned near to our line-of-sight, the pulsation phase will be the same across most of the viewed surface.

The main arguments for depth effects being the principal cause of the amplitude and phase variations are (i) that a radial node is plausibly situated in the observable atmosphere (Gautschy et al. 1998, Appendix A.2), and (ii) that the bisector velocity varies with height in the Hα line. In Section 6.3.3, we discussed the possibility of systematic errors causing the bisector velocity variations. Here, we make a simple calculation to test the accuracy of these velocities below a relative intensity of 0.7 in the line.

For α Cir and HR 3831 (ν_{-1} and ν_{+1}), we averaged the bisector-velocity amplitudes below a height of 0.7 (giving half weight to the amplitudes between 0.6 and 0.7) in order to compare with the cross-correlation measurements. This is a plausible estimate for the cross-correlation because the slope of the Hα profile is steep and nearly constant between 0.4 and 0.6, and is less steep above 0.6. For α Cir, we obtained an estimate of $\sim$170 m s^{-1} while the actual cross-correlation measurements gave 168–182 m s^{-1} (depending on the band, nos. 85–88). For HR 3831, we obtained estimates of $\sim$340 and $\sim$290 m s^{-1} for the two frequencies while the actual measurements gave 338–361 and 296–318 m s^{-1} respectively. The good agreement, between the estimates obtained from the bisector analysis and the velocity amplitudes from the cross-correlation measurements (using four different bands), argues that the bisector velocities are accurate.

However, there is a similarity between the α Cir and HR 3831 bisector results (see Figure 8.2) that is possibly inconsistent with depth effects being the cause of the bisector variations. This is because the pulsations of these two stars have significantly different periods (7 and 12 minutes) and, therefore, have different vertical wavelengths, assuming that the sound speed is approximately the same between their atmospheres. If depth effects are causing the bulk of the observed bisector variations, the Hα line is formed over a larger vertical distance, and/or the sound speed is lower, in the atmosphere of HR 3831.

Again, surface effects could explain the bisector variation in α Cir and HR 3831 if they were pulsating in modes with $\ell \geq 3$ (see Hatzes 1996). Therefore, we are left with two relatively straightforward explanations for the amplitude and phase variations: (i) they pulsate in dipole modes and the variations are caused by depth effects, or (ii) they pulsate in $\ell = 3$ modes and the variations are caused by surface effects. A more complicated explanation could involve a combination of standing waves, running waves, surface effects, distorted modes and blending.

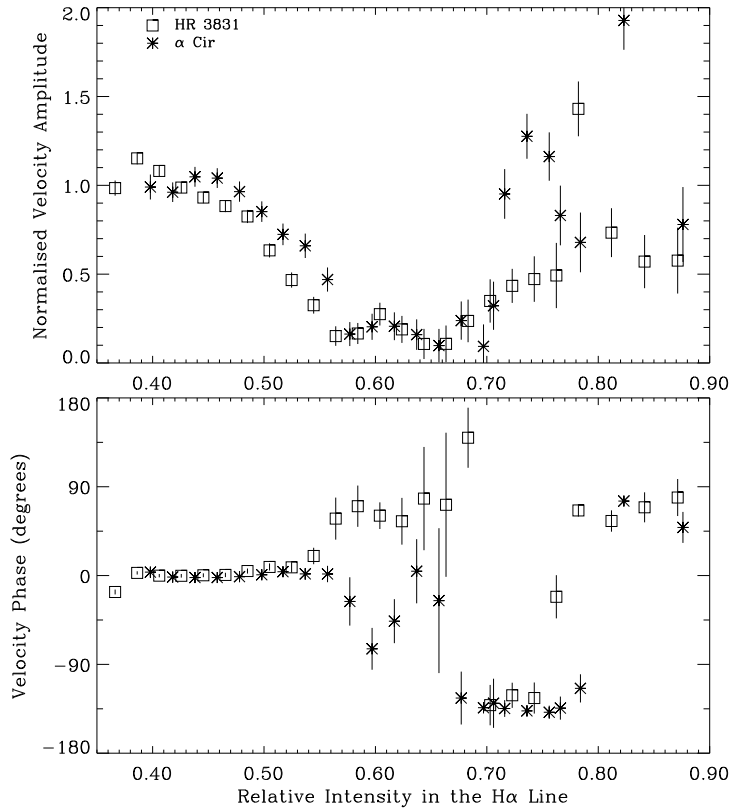

Figure 8.2 Comparison of the Hα bisector variations between HR 3831 and α Cir. This figure is essentially an overplot of Figures 7.10 and 6.2 except, for HR 3831 the measurements for ν_{-1} and ν_{+1} were averaged and, for α Cir the Stromlo and La Silla data were combined. Additionally, the amplitudes were normalised by dividing by an average taken between heights 0.40 and 0.45 (519 m s^{-1} for HR 3831 and 267 m s^{-1} for α Cir) and the phases were shifted.

8.2 Rotational modulation in HR 3831

There are many examples of rotational modulation shown in Chapter 7 and in Appendix B.2. The large variation in the shape of the modulation between different observables was an unexpected result. There are three possible explanations that we will describe here.

(i) The observed frequency triplet is caused by three different modes.

(ii) The oblique pulsator model is accurate and the variations are caused by 'systematic errors' in the measurements.

(iii) The oblique pulsator model is correct but needs to be modified to include effects due to spots or some other mechanism.

In the first case, the relative amplitude between different modes would be expected to vary for different observables. This is the natural explanation for the differences between ν_{-1} and ν_{+1} of the metal-line velocity amplitudes and phases (Figures 7.6 and 7.7) and of the Hα-width amplitudes and phases (Figure 7.11). However, it would require some rotational phase-locking process to account for the frequency separations being equal to the rotation frequency.

In the second case, no simple systematic error could explain the variation in the shape of the rotational modulation. Any such error would need to be varying with the rotation. For instance, a variation in blending could possibly account for the rotational modulation of the metal-line amplitudes and phases, but it could not account for the Hα-width variations.

For the third case, we consider the Hα line because it is the least affected by blending. First, note that the intensity modulation, using a filter with a FWHM of about 6Å, is fitted well by the rotational modulation derived from the photometric triplet (Figure B.18). This means that the *total intensity* variations below a height of about 0.62 are in agreement with the oblique pulsator model. The bisector velocities are also in agreement, so it is just the width variations below 0.62 that are not in agreement with the model. Perhaps this could be explained by hot spots in the upper atmosphere that cause temperature amplitude and phase differences and, as the star rotates, the effect on the Hα profile varies; i.e., a spotted oblique pulsator model.

8.3 Future work

It is clear that the high-resolution study (R$\gtrsim$40000) of different metal lines will be necessary to improve the understanding of the pulsation and the structure of the atmosphere in roAp stars, because of the problems associated with blending at lower resolution ($R \sim 5000$ in this thesis). It will then be possible to compare the velocity amplitudes and phases between different atoms and ionization states. Theoretical work needs to be done to calculate formation depths for individual lines, including the effects of diffusion and the magnetic field. The aim is to build up a coherent picture of the pulsation in the atmosphere.

Of the results on roAp stars in this thesis, the Hα profile measurements are least affected by blending and cannot easily be improved using high-resolution spectroscopy. The profile measurements require a good continuum fit across the Hα line, which is about 100Å wide in these A-stars. For this reason, a spectrum which is stable across at least 400Å is preferable. This is harder to obtain with high-resolution spectroscopy due to the blaze-pattern and the size of CCD detectors. Although improvement could be made on the results using intermediate-resolution spectroscopy ($R \sim$15000), modelling the formation of the Hα line is more important. Determining depth and surface effects on the Hα profile will complement high-resolution spectroscopic and theoretical studies of metal lines.

Photometric oscillation spectra could be considerably improved from observations of roAp stars using small space telescopes. Two such missions plan to include roAp stars as part of a project to measure oscillations in nearby stars (MONS, see Baldry 1998; and MOST, `http://www.astro.ubc.ca/MOST/`). If successful, it will result in the detection of new modes and improved asteroseismology of the brightest roAp stars.

The spectroscopic study of the pulsations in roAp stars has produced more questions than answers, due to the complexity of the observed spectral changes. For the same reason, the 'amount of information' obtainable is very large (e.g., variations in amplitudes and phases) compared to other pulsating stars. Therefore, roAp stars are prime stellar objects for testing diffusion, magnetic field and pulsation theories. In the future, the study of rapidly oscillating Ap stars may proceed rapidly, oscillating between theoretical and observational advances.